Gut microbial interaction networks control autoimmunity to neuroretina

Amy Zhang[1#], Reiko Horai[1#*], Yingyos Jittayasothorn[1], Jonathan H. Badger[2], Zhichao Wu[3], Akriti Gupta[1], Samyuktha Arunkumar[1], Caitlin E. Murphy[1], Guangpu Shi[1], Vijayaraj Nagarajan[1], John A. McCulloch[2], Shilpa Kodati[1], H Nida Sen[1], Jung Wha Lee[1], Jonathan P. Jacobs[4], Xiaoyan Xu[1], Mary J. Mattapallil[1], Zixuan Peng[1], Biying Xu[1], Robert J. Palmer[5], Nadim Majdalani[6], Kenya Honda[7], Colm O'hUigin[2], Rachel R. Caspi[1*]

[1]Laboratory of Immunology, National Eye Institute, National Institutes of Health, Bethesda, MD, USA

[2]Genetics and Microbiome Core, Laboratory of Integrative Cancer Immunology, Center for Cancer Research, National Cancer Institute, National Institutes of Health, Bethesda, MD, USA

[3]Laboratory of Pathology, Center for Cancer Research, National Cancer Institute, National Institutes of Health, Bethesda, MD, USA

[4]Goodman-Luskin Microbiome Center, David Geffen School of Medicine at UCLA, Los Angeles, CA, USA

[5]Structural Biochemistry Unit, National Institute of Dental and Craniofacial Research, National Institutes of Health, Bethesda, MD, USA

[6]Laboratory of Molecular Biology, Center for Cancer Research, National Cancer Institute, National Institutes of Health, Bethesda, MD, USA

[7]Keio University School of Medicine, Tokyo, Japan

[#]Equal contribution

*Correspondence to:

Rachel R. Caspi (caspir@nei.nih.gov)

Laboratory of Immunology, National Eye Institute, National Institutes of Health
10 Center Drive, 10/10N248, Bethesda, MD 20892-1857, USA
or

Reiko Horai (hreiko@nih.gov)

Laboratory of Immunology, National Eye Institute, National Institutes of Health
10 Center Drive, 10/10S243, Bethesda, MD 20892-1857, USA

Funding: NIH/NEI Intramural funding, Project Number EY000184

Commercial Disclosures: None

Running title: Gut microbial interactions drive autoimmune uveitis

KEYWORDS

autoimmune uveitis, T cell receptor transgenic mice, humanized gnotobiotics, fecal microbiota reconstitution, microbial interaction, short chain fatty acids

ABSTRACT

The gut microbiome influences the development of immune-mediated inflammatory diseases. One such condition is autoimmune uveitis, a sight-threatening ocular inflammation driven by retina-specific T cells[1]. Using a model of spontaneous experimental autoimmune uveitis (sEAU) we showed that gut commensals provide innate and adaptive immune stimuli that trigger the disease[2]. Here we report that uveitis-promoting microbes are present in human gut flora and that colonization of germ-free (GF) mice with commensal flora from healthy human donors was sufficient to provoke disease. Severity of sEAU correlated with expansion of Akkermansia and contraction of short-chain fatty acid (SCFA)–producing Firmicutes, as well as decreased SCFA levels and a dominant gut Th1 effector response. Mechanistic gain-of-function experiments, enriching GF sEAU mice with Akkermansia, reproduced these microbiome, metabolite and immune phenotype shifts, and exacerbated disease. We propose that Akkermansia promotes autoimmunity by outcompeting SCFA-producers and enhancing Th1-type responses. Notably, an inverse correlation between Akkermansia (Verrucomicrobia) and Firmicutes was also present in fecal microbiome of patients with uveitis, multiple sclerosis and Crohn's disease. These findings reveal a stereotypic gut microbial interaction network that regulates systemic immune balance, and may represent an ecologically conserved mechanism through which the gut microbiome modulates autoimmune and inflammatory diseases.

INTRODUCTION

Immune-privileged tissues are increasingly recognized as sites where host–microbiota interactions influence immunological balance in autoimmune and inflammatory diseases[3,4]. Multiple mechanisms have been proposed that explain the central role of microbiota in driving inflammation in the central nervous system (CNS), including innate and adaptive effects such as molecular mimicry[2,5], bystander activation[6], epitope spreading[7,8] and dual T cell receptors (TCRs)[9]. Neuroretina of the eye is part of the CNS that represents a quintessential immune-privileged tissue, making it a valuable model to study gut microbiota and autoimmunity in the CNS.

Autoimmune uveitis is a T cell-driven intraocular inflammation of unknown etiology that targets the neuroretina and can lead to blindness[1]. It is represented by the models of experimental autoimmune uveitis (EAU) in animals. EAU is induced in wild type mice by immunization with the retinal antigen IRBP[1], or can develop spontaneously (sEAU) in mice expressing a transgenic IRBP-specific TCR cloned from the immunization induced model (line R161H)[10]. Our previous studies highlight the critical role of gut microbiome in triggering sEAU by providing antigenic stimuli that activate retina-specific T cells[2]. Subsequent research reported inhibitory effects of microbiome depletion also in induced EAU[11], where the antigen is provided, emphasizing the antigen-independent (innate?) effects of gut microbes on EAU. Interestingly, gut microbiome studies in uveitis patients have revealed differences in gut flora between patients and healthy controls[12-16], but mechanistic information could not be resolved.

Because inductive events and causal relationships cannot be studied in patients, we employed the model of sEAU in R161H TCR transgenic mice[10], which may provide a more physiologically relevant system to study triggers delivered by the microbiota. To gain mechanistic insights into how human gut microbiota might affect the development of autoimmune uveitis, we created gnotobiotic breeding colonies of R161H mice harboring healthy human gut flora by reconstituting GF parental mice with fecal material from three healthy human donors. The rationale for focusing on healthy donors is that *(i)* every uveitis patient was once a healthy person, so by definition, uveitis-relevant microbes should be present in the healthy person's gut flora, and *(ii)* the composition of patient

31 flora could have been altered by their disease or by their treatment, confounding data
32 interpretation.

33 Using a multiomic strategy that integrates microbial, metabolomic and immune profiling of
34 human flora (HuFl)-reconstituted R161H mice, combined with analyses of human
35 autoimmune disease datasets, we identified a microbial interaction network comprising
36 an "Akkermansia/Verrucomicrobia—Firmicutes axis" that appears to regulate
37 autoimmunity. Our data points to an underexplored but fundamental mechanism, where
38 interactive relationships in the microbial community play a central role in regulation of
39 autoimmune disease pathogenesis by microbiota[17].

40 **RESULTS**

41 **1. Human gut commensals support development of spontaneous experimental**
42 **autoimmune uveitis (sEAU)**

43 R161H mice harboring mouse microbiota (specific-pathogen-free, SPF) typically develop
44 moderate to severe uveitis with high penetrance (100% incidence by two months of
45 age)[10]. To first assess whether human gut microbiota affect uveitis development, we
46 developed "humanized gnotobiotic" R161H mouse lines as our pre-clinical model, by
47 reconstituting breeding pairs of GF R161H mice with gut microbiota from three healthy
48 human subjects—U, V, and W. Each line was maintained in separate isolators through
49 successive generations, so that the offspring acquired the human flora naturally from
50 their respective parents (Fig. 1a).

51 Microbiome sequencing results showed successful engraftment of human flora in
52 gnotobiotic R161H mice. The succession of gut microbiota through generations of
53 breeding in gnotobiotic isolators did not appear to diminish the differences between
54 individual cohorts, and each U, V, or W mouse recipient cohort preserved the microbial
55 signatures of its original donor (Fig. 1b).

56 Human commensal microbes supported uveitis development in R161H mice. Although
57 HuFl mice displayed a broad spectrum of disease severity scores, the scores were on

average lower than those of SPF mice that harbor normal mouse flora (Fig. 1c & Extended Data Fig. 1a). We did not observe obvious sex differences with respect to disease severity in HuFl mice (Extended Data Fig. 1b). Immune phenotype of colonic $CD4^+$ T cells, based on a range of cell surface and intracellular markers, clearly distinguished HuFl mice from GF and SPF mice (Fig 1d & Extended Data Fig. 1c-e). The HuFl mice showed a spectrum of disease scores and memory marker expression between GF (low) and SPF (high) mice (Fig. 1e), had fewer IFN-γ-producing Th1 and IL-17A-producing Th17 effector cells and more regulatory T cells (Tregs) expressing Foxp3 and IL-10 than did SPF mice (Fig. 1f-g). This immune phenotype was consistent with other activation markers and Th1/Th17 signature molecules (Extended Data Fig. 1e). This phenotype may explain the lower disease scores that they developed.

2. Human flora sEAU tracks with a dominant Th1 phenotype and abundance of Akkermansia (Verrucomicrobia)

Since both Th1 and Th17 effector phenotypes can drive autoimmune uveitis[18-20], we set out to define the immune signatures that associate with disease in the HuFl model. We categorized histological scores into high (score ≥ 1.5), mid (0.75 < score < 1.5), and low (score ≤ 0.75) to facilitate statistical analysis. Interestingly, IFN-γ/T-bet expressing CD4 T cells, rather than IL-17A/RORγt expressing cells, in the gut (and other tissues) associated strongly with severe disease phenotype (Fig. 2a-d). This suggests that uveitis development in HuFl mice is more dependent on Th1 than Th17.

Microbiome analysis of parental and offspring HuFl mice showed that colonized mice adopted only a subset of the original donor taxa (Extended Data Fig. 2a-b). This could be a result from loss during human stool sample preservation and transfer processes, and/or from inefficient engraftment of some non-native microbes to the gut environment of a different host species. However, in terms of the overall microbial composition, each mouse cohort remained closer to their original donor, preserving a distinct microbial footprint (Fig. 1b & Extended Data Fig. 2c-d). Differences between female *vs.* male HuFl mice in terms of microbial abundance and composition were minimal, if any, compared to the differences based on human donors (Extended Data Fig. 2e-f). This is compatible

with the apparent lack of sex differences in disease severity of HuFI mice (Extended Data Fig. 1b).

We then explored how gut microbiome associates with severity of uveitis. Correlational heat map of major bacterial taxa at the family level revealed strong links between several taxa and histology scores (Fig. 2e). Among them, Akkermansia (the only representative of Verrucomicrobia in HuFI mice) correlated with high disease scores (Pearson r = 0.5, FDR <0.05), whereas certain members of the Firmicutes phylum were correlated with low disease scores (Pearson r = -0.3, FDR <0.05). Differential abundance analysis between high and low histology categories consistently showed that Akkermansia was enriched in mice with high disease, whereas Firmicutes (especially Clostridia) were enriched in mice with low disease (Fig. 2f-g & Extended Data Fig. 2g).

3. SCFA signatures are enriched in low disease HuFI mice or healthy subjects

SCFAs are metabolites of commensal gut microbes, especially Firmicutes, resulting from fermentation of dietary fiber, and have anti-inflammatory properties in a range of pathological conditions[21]. Some SCFAs, e.g. butyrate and propionate, may have therapeutic potential in induced EAU[22,23]. In the current study, a key observation from differential abundance analyses of mice with low and high disease scores was that SCFA-producing Firmicutes were associated with lower sEAU scores (Fig. 2e). Therefore, it appeared plausible that SCFAs may also have the potential to modulate sEAU.

To address this, we mined functional gene signatures from shotgun metagenomic sequences of HuFI mice. Genes known to be involved in SCFAs synthesis and metabolism were mapped to the simplified pathways shown in Fig. 3a. Consistent with the observed differences in microbial abundance (Fig. 2e), the genes involved in main SCFA pathways were enriched in mice with low disease scores and reduced in mice with high disease scores (Fig. 3b). In agreement with the pathway analysis, metabolomic quantification of SCFAs in the gut and serum of the mice confirmed that higher disease scores were associated with lower SCFA concentrations both locally and systemically (Fig. 3c).

116 We next examined whether this signature was present in a cohort of uveitis patients seen
117 at the NEI clinic, compared to healthy controls. Because uveitis is a heterogenous
118 disease, we focused on a subset of patients whose disease was restricted to the eye
119 (idiopathic uveitis, sympathetic ophthalmia, birdshot chorioretinopathy, and Vogt-
120 Koyanagi-Harada disease with ocular manifestations), as modeled by EAU. Similarly to
121 the HuFI R161H mice, enzymes involved in acetate, butyrate and propionate pathways
122 (Fig. 3d) and their corresponding SCFAs (Fig. 3e), were reduced in uveitis patients
123 compared to healthy controls. This supports a role for SCFAs in regulation of human
124 uveitis.

125 **4. Akkermansia negatively correlates with Firmicutes in both sEAU and clinical**
126 **uveitis**

127 Among all taxa in HuFI mice, Akkermansia abundance was shown to be a prominent
128 correlate of severe uveitis and IFN-γ-producing CD4+ T cells in the gut (Fig. 2e-f,
129 Extended Data Fig. 3a–b), whereas SCFA-producing Firmicutes were reduced in the
130 same animals (Fig. 2e, g). We therefore analyzed their relative abundance and potential
131 interdependence to determine whether competitive interactions between these taxa might
132 contribute to autoimmune uveitis.

133 We first quantified abundance of Akkermansia and Firmicutes, and found them to be
134 inversely correlated (Fig. 4a). An in-depth computational analysis of the bacterial
135 association network confirmed the negative correlation between Akkermansia and
136 multiple families of SCFA-producing Firmicutes (Fig. 4b, Extended Data Fig. 3c). Levels
137 of major SCFAs in feces also exhibited an inverse correlation with Akkermansia
138 abundance (Fig. 4c). Taken together, this supports an interpretation of a negative
139 interaction between Akkermansia and a range of SCFA-producing microbes.

140 Similarly, gut microbiome interaction networks of uveitis patients displayed a negative
141 relationship between Verrucomicrobia (primarily Akkermansia) and SCFA-producing
142 Firmicutes (Clostridia, class level), but this relationship was not evident in healthy
143 subjects (Fig. 4d). This supports the relevance of the sEAU model to clinical disease.

144 **5. Akkermansia promotes uveitis by outcompeting SCFA producers and**
145 **decreasing circulating SCFA levels**

146 To validate the proposed microbiome interaction network *in vivo*, we used a gain-of-
147 function approach, where GF R161H mice received Akkermansia alone or Akkermansia
148 mixed with HuFI mouse donor fecal flora. In the first paradigm, we associated GF mice *de*
149 *novo* with cultured *Akkermansia muciniphila* (the type species of Akkermansia) or with
150 sterile PBS as control, and maintained them in static microisolators using facility-standard
151 "sterile handling" techniques, designed to minimize environmental microbial exposure
152 (Extended Data Fig. 4a). This approach resulted in a minimal gut microbial population of
153 very low diversity (≤10 total detectable taxa/mouse), dominated by Verrucomicrobia
154 (Akkermansia) and Firmicutes (Extended Data Fig. 4b-d).

155 First paradigm: A single oral gavage led to successful and sustained engraftment of
156 Akkermansia, and resulted in higher uveitis scores (Extended Data Fig. 4e-f). Akkermansia
157 was nearly undetectable in the PBS control group, whose gut microbiota became
158 dominated by Firmicutes (Extended Data Fig. 4g). As such, the relative abundances of
159 Akkermansia and Firmicutes showed a near-perfect inverse relationship (r-squared > 0.99,
160 $p < 0.0001$) (Extended Data Fig. 4h). Other bacterial phyla that are prominent in normal
161 mouse or human gut flora were low or on the borderline of detectability (Extended Data
162 Fig. 4i). Thus, this model reflects a minimal-diversity gut ecosystem dominated by the two
163 taxa that we hypothesize to display competitive dynamics that control expression of
164 disease.

165 Second paradigm: To examine this hypothesis under more physiological conditions, where
166 Akkermansia is not given a major "head start", we associated GF R161H mice with flora
167 from HuFI mice (selected for low disease and low abundance of Akkermansia) "spiked", or
168 not, with cultured *A. muciniphila* (Fig. 5a). Fecal microbiome profiling confirmed successful
169 microbial engraftment and stability of Akkermansia-high or Akk-low status (Fig. 5b &
170 Extended Data Fig. 5a). Akkermansia "spiked" flora induced more severe uveitis than base
171 HuFI alone (Fig. 5c) and the relative abundances of Akkermansia and Firmicutes were
172 consistently inversely correlated (Fig. 5d). Notably, among the major bacterial phyla,

173 Firmicutes was the only phylum whose abundance was decreased in Akk-enriched mice
174 (Fig. 5b & Extended Data Fig. 5b), particularly those taxa considered "professional" SCFA
175 producers such as Clostridia[24] (Extended Data Fig. 5c). To confirm that the effects
176 described above were indeed Akkermansia-specific, we associated GF R161H mice with
177 the same HuFl "spiked" with *E. coli*. The disease-promoting phenotype and the reduction in
178 Firmicutes abundance were not recapitulated, supporting the notion that the observed
179 effects were specific to Akkermansia (Extended Data Fig. 5d-f). Together, these results
180 reinforce a dynamic balance between Akkermansia and Firmicutes that modulates
181 autoimmune uveitis in a physiologically relevant setting.

182 To mechanistically link Akkermansia–Firmicutes dynamics with circulating SCFA levels
183 available to regulate uveitis-relevant immune responses, we measured serum SCFAs and
184 host immune parameters. All three major SCFAs – acetic, butyric and propionic acids –
185 were reduced in Akk-high mice compared with Akk-low mice (Fig. 5e), consistent with the
186 negative relationship between Akkermansia and Firmicutes. This reduction was not
187 observed in the *E.coli* control group (Extended Data Fig. 5g). Given the known
188 immunomodulatory role of SCFAs[21], we examined whether this metabolomic shift was
189 associated with an altered systemic effector response. In both the Akk-associated minimal
190 flora model and the Akk-enriched HuFl model, reduced serum SCFAs were tightly coupled
191 with elevated serum and/or gut IFN-γ responses (Fig. 5f-i). These results imply that SCFAs
192 may regulate disease by dampening the Th1 effector response.

193 The final mechanistic question was whether Akkermansia can provide surrogate antigenic
194 stimuli to trigger activation of the R161H TCR-expressing cells in the gut[2]. To address this,
195 we used an *in vitro* activation assay, where naïve R161H CD4 T cells and antigen-
196 presenting cells were cultured with Akk-rich HuFl gut content extracts, or with heat-killed
197 Akkermansia. Unlike SPF gut flora extracts or the cognate peptide antigen[2,10], neither
198 Akkermansia preparation activated the retina-specific T cells, as measured by expression
199 of CD69 and Nur77 (Extended Data Fig. 6a-b), indicating that Akkermansia was not acting
200 as an antigen mimic.

201 Single cell RNA-seq analysis of colonic CD4 T cells, of which an average of 15%
202 expressed the R161H TCR, revealed that both R161H TCR-expressing and non-R161H
203 (endogenous) T cells had a Th1, rather than a Th17, signature, that positively correlated
204 with abundance of Akkermansia (Extended Data Fig. 6c-d). Thus, Akkermansia appears
205 to skew the T cell response phenotype independently of the T cell antigen specificity,
206 which for non-R161H cells could be other gut microbes or food antigens. VDJ analysis
207 did not reveal evidence for a 2nd TCR among R161H TCR+ cells. In addition, *in silico*
208 analysis did not reveal shared sequence(s) between Akkermansia and IRBP$_{161\text{-}180}$, which
209 is the cognate R161H TCR epitope. We interpret this to mean that Akkermansia
210 regulates disease through innate, adjuvant-like mechanisms that shape the T-cell effector
211 response phenotype, as well as indirectly by modulating SCFA-producing Firmicutes.
212 This working model is depicted in Figure 6a.

213 **6. The inverse relationship between Verrucomicrobia and Firmicutes extends to**
214 **clinical uveitis, multiple sclerosis and Crohn's disease**

215 Because effector Th1 skewing in the Akk-rich gut environment was independent of
216 antigenic specificity, we hypothesized that it could be associated with human
217 inflammatory conditions, such as uveitis, multiple sclerosis (MS) and inflammatory bowel
218 disease (IBD). To establish a common metric for comparing healthy to diseased state, we
219 used the phylum-level ratio of Verrucomicrobia / Firmicutes (V/F ratio) which consistently
220 tracked with disease severity in HuFI mice (Fig. 6b). Application of this metric to the entire
221 cohort of our clinical uveitis samples (so as to minimize any selection bias), revealed
222 higher V/F ratios in uveitis patients compared to healthy subjects (Fig. 6c). We next
223 examined publicly available MS[25] and IBD[26] datasets, the latter comprising patients with
224 Crohn's disease and ulcerative colitis (UC). Compared to healthy controls, the V/F ratio in
225 MS, and in Crohn's disease patients—a condition predominantly driven by Th1-mediated
226 inflammation—but not in UC patients[27,28], was markedly elevated (Fig. 6c). Notably, the
227 ratio of Firmicutes / Bacteroidetes (F/B ratio), commonly used as a broad indicator of
228 "dysbiosis" [38], has not consistently distinguished patients from healthy controls across
229 disease settings (Fig. 6c). Taken together, the gut microbial interaction networks
230 indicated a negative correlation of Verrucomicrobia (Akkermansia) with Firmicutes not

231 only in R161H mice, but also in uveitis, MS and Crohn's disease patients, supporting the
232 generality of this relationship.

233 **DISCUSSION**

234 In this study, we report a gut microbial interaction network that regulates autoimmune and
235 inflammatory processes along the "gut–eye axis". By integrating data-driven analyses
236 and *in vivo* microbial perturbation, we provide compelling evidence for a negative
237 relationship between Akkermansia and Firmicutes and link it to disease severity.
238 Specifically, Akkermansia appears to promote sEAU in HuFl R161H mice by
239 outcompeting SCFA-producing Firmicutes in the gut, resulting in diminished SCFA levels
240 and enhanced Th1 responses both locally and systemically (Fig. 6a). Our findings
241 provide a mechanistic basis for how the gut microbiome controls ocular autoimmunity,
242 dissect the complex interacting stimuli that underpin this process, and highlight its broadly
243 generalizable nature.

244 Our network-based perspective contrasts with previous studies, which have mostly
245 focused on how individual gut microbial taxa influence disease and host immunity[4].
246 *A. muciniphila* has been studied across a spectrum of inflammatory and autoimmune
247 diseases, and different reports have described inconsistent functional effects[29]. As an
248 example, although Akkermansia promoted Th1 polarization of human PBMCs[30] and
249 positively correlated with disease activity in MS patients[25,30-32], *in vivo* Th1-polarizing
250 activity was not observed in Akk-monocolonized mice[30] and in the context of a diverse
251 gut microbiome (SPF mice), Akkermansia-specific T cells differentiated into a mixture of
252 effector phenotypes[33]. Our finding that Akkermansia affects sEAU through interactions
253 that modulate the gut microbial network explains and reconciles these contradictions by
254 demonstrating that the immunological impact of Akkermansia—and probably of any
255 single microbe in general—is a product of its interactions with the broader gut microbial
256 community.

257 The R161H sEAU model provides a platform to dissect these contextual effects. When
258 the model was first established, we identified signaling by a (microbiota-dependent)

259 mimic antigen in the SPF flora of R161H mice as an important, but possibly not the only,
260 disease trigger[2]. In the "humanized" sEAU mice, Akkermansia does not appear to act as
261 a surrogate antigen, suggesting that other HuFl members may provide this function.
262 However, we did not attempt to identify the HuFl microbial mimic, as identifying it would
263 lack translational relevance. The R161 TCR recognizes a mouse class II (I-A^r)-restricted
264 epitope of IRBP. Human MHC class II molecules would almost certainly present a
265 different epitope(s) from any given antigen than does mouse I-A^r, plus the epitope(s)
266 would differ between individuals, given the heterogeneity of human MHC haplotypes.
267 Moreover, whereas IRBP is a dominant retinal autoantigen in mice, human uveitis more
268 commonly involves recall responses to arrestin[1]. Therefore, although the HuFl R161H
269 sEAU model cannot reveal specific antigenic targets involved in human uveitis, it can
270 reveal conserved mechanisms shared across species, such as the microbial interaction
271 network identified in this study.

272 A key feature of this microbial network is the negative relationship between Akkermansia
273 and Firmicutes, which links gut microbial composition to systemic inflammation. This
274 antagonism likely arises from multiple, non-mutually exclusive mechanisms. Both taxa
275 are dominant colonizers of the colon and may engage in direct niche competition and
276 indirect interactions. Akkermansia promotes mucus degradation during gut
277 inflammation[34,35]. The compromised mucus barrier would exacerbate inflammation and
278 oxidative stress[36], creating inhospitable conditions for obligate anaerobes like Firmicutes.
279 Finally, while Akk antagonizes SCFA-producing Firmicutes, their SCFAs can in turn act to
280 suppress Akkermansia growth and mucolytic activity[37].

281 All those interactions are reflected in the V/F ratio, which may serve as an indicator of
282 inflammatory state and immune polarization across species, supporting its translational
283 value. A similar "legacy" metric F/B ratio has been used to indicate overall shifts in gut
284 microbiome composition, but is now being phased out due to its inconsistent disease
285 associations[38,39]. We propose that the V/F ratio is more specifically informative in
286 autoimmune and inflammatory settings. Of note, numerous studies report an association
287 between uveitic diseases and gut inflammation. Uveitis is associated with an increased
288 risk of Crohn's (but not of UC)[40], and Crohn's patients are more likely than UC patients to

develop uveitis[41]. The findings are compatible with the notion that the V/F ratio increases under conditions where gut inflammation co-occurs with extraintestinal autoimmunity. The V/F ratio may also rise under Th1-dominant inflammatory conditions, as observed in our data. Our analyses reveal elevated V/F ratios not only in our patients with uveitis, but also in published datasets from patients with MS[25] and IBD[26]. Within IBD, increases in V/F were evident in Crohn's disease (Th1-dominant[42-44]), but not in UC (Th2-like[45-47]).

Limitations of the study: The complexity of the Akkermansia–Firmicutes axis poses a major challenge to resolving microbial relationships at species and strain levels. Emerging approaches such as bacterial spatial transcriptomics[48] are not yet sufficiently developed to define the precise mechanisms by which Akkermansia antagonizes SCFA-producing Firmicutes. In addition, the finite capacity of our GF R161H colony constrains the scale and breadth of gnotobiotic experiments. Consequently, several mechanistic studies, including administering individual SCFAs to HuFI mice for functional validation, could not be completed within a feasible time frame.

In conclusion, our findings show that a complex microbial interaction network—rather than individual taxa—plays a central role in shaping the gut–eye axis. The Akkermansia–Firmicutes relationship, captured in a simple translational metric (the V/F ratio) that tracks inflammatory state and immune polarization, likely reflects a generalizable ecological principle in which microbial competition influences systemic immune balance and susceptibility to autoimmunity and inflammation, and which extends across species. Future studies aimed at defining the mechanisms by which Akkermansia gains an advantage over SCFA-producing Firmicutes, may guide the development of microbiome-based interventions for autoimmune and inflammatory diseases that intersect with gut dysregulation.

315 **METHODS**

316 ***Mice.*** R161H mice on the B10.RIII background[10] were bred in-house and maintained
317 under SPF conditions and fed standard facility chow *ad libitum*. GF and HuFl R161H
318 mice were maintained in the gnotobiotic isolators. The animal study protocol (NEI-688)
319 was approved by the NEI Institutional Animal Care and Use Committee.

320 ***Generation of gnotobiotic mice with human stool samples.*** Human stool samples of
321 healthy volunteers were collected at Keio University according to the study protocol[49]
322 approved by the Institutional Review Boards (approval number 20150075) and informed
323 consent was obtained from each subject. Stool samples were suspended in 20% glycerol
324 in PBS, snap frozen in liquid nitrogen and stored at -80°C. The U, V, and W stocks were
325 thawed and gavaged into GF R161H mice and individual cohort lines were established in
326 separate germ-free isolators.

327 ***Evaluation of uveitis phenotype.*** Development of uveitis was monitored by fundoscopic
328 observation via a binocular microscope of anesthetized mice at the indicated age. For
329 histopathology, eyes were enucleated and fixed in 4% glutaraldehyde for 1 h and
330 transferred to 10% formaldehyde for additional 24 h, embedded in methacrylate, and
331 processed for H&E staining. Disease scores of fundoscopy and histology were assigned
332 by a masked observer on a scale of 0–4, according to the criteria for EAU scoring
333 described in detail elsewhere which are based on the number, size and type of lesions[50].

334 ***HuFl R161H fecal suspension preparation.*** Cecal and colonic contents from HuFl mice
335 of varying disease severity were collected under sterile conditions and immediately
336 transferred on ice to an anaerobic chamber (Coy Laboratory Products). Contents were
337 filtered three times through a 70 μm cell strainer in 20% glycerol–PBS, and aliquoted to
338 prevent repeated freeze–thaw cycles. Each sample was prepared from either individual
339 mice or pools of mice with the same disease severity. The baseline HuFl suspension for
340 reconstitution experiments was prepared from two mice with low uveitis scores and
341 validated by 16S sequencing to contain ~1% Akkermansia (ranges 1–8% in tested
342 samples).

343 ***In vivo microbial enrichment by gnotobiotic reconstitution.*** *A. muciniphila* or *E. coli*
344 were cultured in mucin-BHI media inside the anaerobic chamber or in LB media in the
345 aerobic incubator, respectively. Microbial monoculture was prepared in advance and the
346 first passage timed to reach the exponential growth phase immediately prior to oral
347 gavage. On the day of gavage, GF R161H were transferred from the gnotobiotic isolators
348 to sterile and static microisolator cages with a Reemay filter top. Using sterile techniques,
349 these mice were examined by fundoscopy and assigned to experimental or control
350 groups based on initial uveitis disease scores, age and sex. While mice were recovering
351 from anesthesia, gavage material was prepared inside the anaerobic chamber for *A.*
352 *muciniphila* or in the aerobic bacterial hood for *E. coli*, or sterile PBS, which in the "HuFI
353 base model" was combined with the selected HuFI fecal suspension, so each mouse in
354 the experimental group would receive an additional ~10^8 CFU of the microbe of interest in
355 200uL HuFI fecal suspension via oral gavage. Fecal sampling and fundoscopy scoring
356 were performed on a weekly basis, and mice were handled under sterile protocols, with
357 cages opened only inside a biosafety cabinet.

358 ***Fecal DNA extraction and quantification of microbes.*** Fecal pellets were collected
359 from individual mice, immediately frozen on dry ice and stored at -80°C until bacterial
360 DNA extraction in house as previously described[51] or by the NCI Genetics and
361 Microbiome Core. Absolute abundance of bacteria in each fecal sample was assessed by
362 quantitative polymerase chain reaction (qPCR) using Akkermansia or *E. coli* standard
363 curves with Fast SYBR Green Supermix (Applied Biosystems, Waltham, MA, USA) and
364 run on a QuantStudio™ 7 Pro Real-Time PCR System (Applied Biosystems). Specific
365 primers for Akkermansia were Akk.mu3.Fwd (5'-
366 GCGTAGGCTGTTTCGTAAGTCGTGTGTGAAAG-3') and Akk.mu3.Rvs (5'-
367 GAGTGTTCCCGATATCTACGCATTTCA-3')[52], and for *E. coli* were Uni515F (5'-
368 GTGCCAGCMGCCGCGGTAA-3') and Ent826R (5'-
369 GCCTCAAGGGCACAACCTCCAAG-3')[53]. Five ng of fecal DNA was amplified per 10 µL
370 reaction with the following cycling conditions: initial denaturation at 95 °C for 20 sec,
371 followed by 40 cycles of 95 °C for 3 sec and 63 °C for 30 sec. A melt-curve analysis was
372 included at the end of each run to confirm amplification specificity. Bacterial counts (CFU)

373 per 5 ng of DNA were extrapolated from fitted standard curves correlating Cq values with
374 bacterial quantity.

375 ***16S rRNA gene sequencing and analyses.*** Fecal samples were processed at the NCI
376 Genetics and Microbiome Core for 16S rRNA gene sequencing as detailed in prior
377 work[51]. 16S amplicon sequence variants (ASV) were inferred with YAMS16 v1.7
378 (https://github.com/jhbadger/YAMS16), a pipeline running DADA2[54], and taxonomically
379 classified using the SILVA reference database (release 138.1)[55]. Microbial diversity,
380 differential abundance and multivariable association analyses were performed with
381 phyloseq v1.42.0[56], MaAsLin2 v1.12.0[57], microViz v0.12.3[58], and custom scripts in R.
382 Microbial association networks were analyzed with NetCoMi[59]. (NCBI SRA submission in
383 progress)

384 ***Shotgun metagenomic sequencing and analyses.*** Selected DNA samples were
385 submitted to CosmosID, Inc. (Germantown, MD, USA) for shallow shotgun sequencing (3
386 million reads per sample). Specifically, DNA libraries were generated using the Nextera
387 XT DNA Library Preparation Kit (Illumina, Inc., San Diego, CA, USA) and IDT Unique
388 Dual Indexes, with total input of 1 ng DNA. Genomic DNA was enzymatically fragmented
389 according to the manufacturer's guidelines, after which unique dual indexes were added
390 to each sample and libraries were amplified through 12 PCR cycles. The products were
391 purified with AMpure magnetic Beads (Beckman Coulter, Inc., Brea, CA, USA) and eluted
392 in EB buffer (QIAGEN). Library concentrations were determined using a Qubit 4
393 fluorometer with a Qubit™ dsDNA HS Assay Kit, and final libraries were sequenced in
394 paired-end mode (2x150 bp) on the Element AVITI platform. JAMS v1.9.9[60] and
395 HUMAnN v3.9[61] were used for taxonomic and functional profiling, and genes involved in
396 metabolic pathways of the main SCFAs (acetate, butyrate and propionate) were identified
397 based on InterPro, Gene Ontology and Pfam annotations, and those present in the
398 uveitis datasets were compared between diseased and healthy groups. (NCBI SRA
399 submission in progress)

400 ***Targeted metabolomics and cytokine quantification.*** Cecal and colonic contents
401 (collectively referred to as "fecal contents"), eyes, and serum were collected from age-

402 matched mice at harvest. Eyes were fixed for histological analysis as described above.
403 Fecal and serum samples were snap-frozen on dry ice and stored at −80 °C. For
404 metabolite profiling, at least 100 mg of fecal contents and 150 µL of serum per mouse
405 were transferred to designated tubes and shipped on dry ice to Metabolon, Inc.
406 (Morrisville, NC, USA) for absolute quantification of eight short-chain fatty acids (acetic,
407 propionic, butyric, isobutyric, 2-methylbutyric, valeric, isovaleric, and hexanoic acids).
408 Serum cytokine concentrations were measured using the Mouse Inflammation Panel (13-
409 plex, LEGENDplex™, BioLegend, San Diego, CA, USA) according to the manufacturer's
410 instructions. Data were acquired on a CytoFlex LX flow cytometer (Beckman coulter) and
411 analyzed with LEGENDplex Data Analysis Software (BioLegend) to quantify cytokine
412 levels based on standard curves.

413 ***Tissue harvesting and flow cytometry analyses.*** Peripheral lymphoid tissues
414 (submandibular lymph nodes, spleen, peripheral lymph nodes, mesenteric lymph nodes),
415 and gut lamina propria from small intestine and colon were collected and prepared for
416 single cell suspensions as described elsewhere[2]. Cells were stained with fluorochrome-
417 conjugated antibodies from BD Biosciences, BioLegend or Thermo Fisher Scientific, and
418 viability dyes from Beckman Coulter. Fluorescence-activated cell sorting analyses were
419 done using CytoFlex LX (Beckman coulter). FlowJo v10 (BD Biosciences) was used for
420 data analyses.

421 ***In vitro activation assay on retina-specific T cells.*** IRBP-specific T cells were
422 harvested from spleen and peripheral lymph nodes of *Tcra*$^{-/-}$ *Nr4a1*^{EGFP} (Nur77^{GFP})
423 R161H mice and were enriched for naïve CD4^{+} cells by negative selection (EasySep,
424 StemCell Technologies). CD11c^{+} dendritic cells were purified from spleen WT B10.RIII
425 mice (Miltenyi Biotec) as antigen-presenting cells. T cells and dendritic cells were co-
426 cultured at a 4:1 ratio in the presence of heat-killed *A. muciniphila*, heat-killed *E. coli*, or
427 bacteria-rich extracts. T cell activation was assessed after 22 h by flow cytometric
428 analysis of CD69 and Nur77 expression.

429 ***5' single cell RNAseq sample processing.*** Colon LP cells were labeled with anti-
430 mouse TotalSeqC-HashTags and cell surface antibodies, and sorted for live CD45^{+} and

431 $CD4^+$ populations using FACSAria III/Fusion sorters (BD Biosciences). Post-sort viability
432 exceeded 80%, and hash-tagged samples were pooled at equal ratios within each
433 experimental group, combining $CD45^+$ and $CD4^+$ fractions at 1:1 ratio to enrich for $CD4^+$
434 T cells. Pooled cells were resuspended in PBS with 0.04% BSA and loaded onto a 10x
435 Genomics Chromium X instrument at 700–1200 cells/μL for single cell 5' gene expression
436 and TCR profiling. Libraries were prepared using the Chromium Next GEM Single Cell 5'
437 Reagent Kits v2 (Dual Index) following the manufacturer's protocol, and sequenced on
438 NovaSeq 6000 platform (Illumina, Inc., San Diego, CA, USA).

439 ***Single cell RNAseq data analyses.*** Sequencing data were processed with Cell Ranger
440 v9.0.1 (10x Genomics) for demultiplexing and alignment to the Mus musculus reference
441 (GRCm39, Genome Reference Consortium, 2024). Cell doublets were detected and
442 removed using Scrublet v0.2.3[62]. Cells exhibiting high mitochondrial transcript content (≥
443 5%) or abnormal gene counts (< 500 or > 8000) were excluded. Expression data were
444 log-normalized and scaled using the Scanpy v1.11.0[63] in Python v3.10. Dimensionality
445 reduction was performed using Principal Component Analysis (PCA) followed by Uniform
446 Manifold Approximation and Projection (UMAP), and cell clusters were identified with the
447 Leiden algorithm[64]. Cell type annotation was based on computational classification using
448 SingleR v2.8.0[65] with mouse immune reference data from celldex::ImmGenData v1.16.0
449 in R v4.4, as well as the expression of canonical cell type marker genes, and validated by
450 cell lineage–specific surface antibody. The expression of both Trav16 and Trbv5 in a CD4
451 T cell was the standard used to identify IRBP-specific T cells[10]. (NCBI SRA and GEO
452 submission in progress)

453 ***NEI clinical samples and public human data.*** Stool samples were obtained from
454 patients with autoimmune uveitis and healthy controls enrolled in a clinical cohort at the
455 National Eye Institute (NEI), National Institutes of Health (NIH). All participants provided
456 written informed consent under the protocol approved by the Institutional Review Board
457 (Protocol 13-EI-0072). A stratified cohort of treatment-naïve autoimmune uveitis was
458 selected for in-depth gut microbial network analysis, representing primarily posterior- and
459 pan-uveitis cases and ocular-restricted phenotypes such as idiopathic uveitis,
460 sympathetic ophthalmia and birdshot chorioretinopathy. 16S rRNA gene and shotgun

metagenomic sequencing of human fecal samples were performed by the Microbiome Cores at the NCI and the Goodman-Luskin Microbiome Center (Los Angeles, CA, USA). Public microbiome data of IBD patients' stool are from PRJNA1198911[26], and that of MS patient stool from the International MS Microbiome Study (iMSMS)[25].

Statistical analyses. Statistical analyses were conducted with R v4.4, Python v3.10, and GraphPad Prism v10.5.0. Non-parametric tests such as Mann-Whitney U and Kruskal-Wallis tests were used for most comparisons between two or more groups. Group differences in multivariate community structure were evaluated by Permutational Multivariate Analysis of Variance (PERMANOVA). Pearson's or Spearman's rank correlation, as well as multivariable association (MaAsLin2 and equivalent methods) were used to assess associations between microbial features and disease or immune phenotypes. P-values were adjusted for multiple comparisons using the false discovery rate (FDR) where applicable, and statistical significance was indicated as follows: * $P < 0.05$, ** $P < 0.01$, *** $P < 0.001$, and **** $P < 0.0001$. Data in bar plots are presented as mean values ± SEMs.

REFERENCES

1 Caspi, R. R. A look at autoimmunity and inflammation in the eye. *J Clin Invest* **120**, 3073-3083 (2010).

2 Horai, R. *et al.* Microbiota-Dependent Activation of an Autoreactive T Cell Receptor Provokes Autoimmunity in an Immunologically Privileged Site. *Immunity* **43**, 343-353 (2015).

3 Horai, R. & Caspi, R. R. Microbiome and Autoimmune Uveitis. *Front Immunol* **10**, 232 (2019).

4 Salvador, R., Zhang, A., Horai, R. & Caspi, R. R. Microbiota as Drivers and as Therapeutic Targets in Ocular and Tissue Specific Autoimmunity. *Front Cell Dev Biol* **8**, 606751 (2020).

5 White, Z. *et al.* Gut inflammation promotes microbiota-specific CD4 T cell-mediated neuroinflammation. *Nature* **643**, 509-518 (2025).

6 Lee, H. G. *et al.* Pathogenic function of bystander-activated memory-like CD4(+) T cells in autoimmune encephalomyelitis. *Nat Commun* **10**, 709 (2019).

7 Miller, S. D. *et al.* Persistent infection with Theiler's virus leads to CNS autoimmunity via epitope spreading. *Nat Med* **3**, 1133-1136 (1997).

8 Deeg, C. A., Amann, B., Raith, A. J. & Kaspers, B. Inter- and intramolecular epitope spreading in equine recurrent uveitis. *Invest Ophthalmol Vis Sci* **47**, 652-656 (2006).

494 9 Ji, Q., Perchellet, A. & Goverman, J. M. Viral infection triggers central nervous system
495 autoimmunity via activation of CD8+ T cells expressing dual TCRs. *Nat Immunol* **11**, 628-
496 634 (2010).
497 10 Horai, R. *et al.* Breakdown of immune privilege and spontaneous autoimmunity in mice
498 expressing a transgenic T cell receptor specific for a retinal autoantigen. *J Autoimmun* **44**,
499 21-33 (2013).
500 11 Nakamura, Y. K. *et al.* Gut Microbial Alterations Associated With Protection From
501 Autoimmune Uveitis. *Invest Ophthalmol Vis Sci* **57**, 3747-3758 (2016).
502 12 Shimizu, J. *et al.* Bifidobacteria Abundance-Featured Gut Microbiota Compositional
503 Change in Patients with Behcet's Disease. *PLoS One* **11**, e0153746 (2016).
504 13 Huang, X. *et al.* Gut Microbiota Composition and Fecal Metabolic Phenotype in Patients
505 With Acute Anterior Uveitis. *Invest Ophthalmol Vis Sci* **59**, 1523-1531 (2018).
506 14 Kalyana Chakravarthy, S. *et al.* Dysbiosis in the Gut Bacterial Microbiome of Patients with
507 Uveitis, an Inflammatory Disease of the Eye. *Indian J Microbiol* **58**, 457-469 (2018).
508 15 Ye, Z. *et al.* A metagenomic study of the gut microbiome in Behcet's disease. *Microbiome*
509 **6**, 135 (2018).
510 16 Ye, Z. *et al.* Altered gut microbiome composition in patients with Vogt-Koyanagi-Harada
511 disease. *Gut Microbes* **11**, 539-555 (2020).
512 17 Steimle, A. *et al.* Gut microbial factors predict disease severity in a mouse model of
513 multiple sclerosis. *Nat Microbiol* **9**, 2244-2261 (2024).
514 18 Luger, D. *et al.* Either a Th17 or a Th1 effector response can drive autoimmunity:
515 conditions of disease induction affect dominant effector category. *J Exp Med* **205**, 799-
516 810 (2008).
517 19 Damsker, J. M., Hansen, A. M. & Caspi, R. R. Th1 and Th17 cells: adversaries and
518 collaborators. *Ann N Y Acad Sci* **1183**, 211-221 (2010).
519 20 Horai, R. & Caspi, R. R. Cytokines in autoimmune uveitis. *J Interferon Cytokine Res* **31**, 733-
520 744 (2011).
521 21 Mann, E. R., Lam, Y. K. & Uhlig, H. H. Short-chain fatty acids: linking diet, the microbiome
522 and immunity. *Nat Rev Immunol* **24**, 577-595 (2024).
523 22 Nakamura, Y. K. *et al.* Short chain fatty acids ameliorate immune-mediated uveitis
524 partially by altering migration of lymphocytes from the intestine. *Sci Rep* **7**, 11745 (2017).
525 23 Chen, X. *et al.* Sodium butyrate regulates Th17/Treg cell balance to ameliorate uveitis via
526 the Nrf2/HO-1 pathway. *Biochem Pharmacol* **142**, 111-119 (2017).
527 24 Louis, P. & Flint, H. J. Formation of propionate and butyrate by the human colonic
528 microbiota. *Environ Microbiol* **19**, 29-41 (2017).
529 25 iMSMS Consortium. Gut microbiome of multiple sclerosis patients and paired household
530 healthy controls reveal associations with disease risk and course. *Cell* **185**, 3467-3486
531 e3416 (2022).
532 26 Orejudo, M. *et al.* Exploration of fecal microbiota in newly diagnosed patients with
533 inflammatory bowel disease using shotgun metagenomics. *Front Cell Infect Microbiol* **15**,
534 1595884 (2025).
535 27 Strober, W., Fuss, I. & Mannon, P. The fundamental basis of inflammatory bowel disease.
536 *J Clin Invest* **117**, 514-521 (2007).

537 28 Guan, Q. A Comprehensive Review and Update on the Pathogenesis of Inflammatory
538 Bowel Disease. *J Immunol Res* **2019**, 7247238 (2019).
539 29 Cani, P. D., Depommier, C., Derrien, M., Everard, A. & de Vos, W. M. Akkermansia
540 muciniphila: paradigm for next-generation beneficial microorganisms. *Nat Rev*
541 *Gastroenterol Hepatol* **19**, 625-637 (2022).
542 30 Cekanaviciute, E. *et al.* Gut bacteria from multiple sclerosis patients modulate human T
543 cells and exacerbate symptoms in mouse models. *Proc Natl Acad Sci U S A* **114**, 10713-
544 10718 (2017).
545 31 Berer, K. *et al.* Gut microbiota from multiple sclerosis patients enables spontaneous
546 autoimmune encephalomyelitis in mice. *Proc Natl Acad Sci U S A* **114**, 10719-10724
547 (2017).
548 32 Jangi, S. *et al.* Alterations of the human gut microbiome in multiple sclerosis. *Nat*
549 *Commun* **7**, 12015 (2016).
550 33 Ansaldo, E. *et al.* Akkermansia muciniphila induces intestinal adaptive immune responses
551 during homeostasis. *Science* **364**, 1179-1184 (2019).
552 34 Desai, M. S. *et al.* A Dietary Fiber-Deprived Gut Microbiota Degrades the Colonic Mucus
553 Barrier and Enhances Pathogen Susceptibility. *Cell* **167**, 1339-1353 e1321 (2016).
554 35 Tingler, A. M. & Engevik, M. A. Breaking down barriers: is intestinal mucus degradation by
555 Akkermansia muciniphila beneficial or harmful? *Infect Immun* **93**, e0050324 (2025).
556 36 Sugihara, K. *et al.* Mucolytic bacteria license pathobionts to acquire host-derived
557 nutrients during dietary nutrient restriction. *Cell Rep* **40**, 111093 (2022).
558 37 Schwabkey, Z. I. *et al.* Diet-derived metabolites and mucus link the gut microbiome to
559 fever after cytotoxic cancer treatment. *Sci Transl Med* **14**, eabo3445 (2022).
560 38 Magne, F. *et al.* The Firmicutes/Bacteroidetes Ratio: A Relevant Marker of Gut Dysbiosis
561 in Obese Patients? *Nutrients* **12** (2020).
562 39 Walters, W. A., Xu, Z. & Knight, R. Meta-analyses of human gut microbes associated with
563 obesity and IBD. *FEBS Lett* **588**, 4223-4233 (2014).
564 40 Lo, T. C., Chen, Y. Y. & Chen, H. H. Risk of inflammatory bowel disease in uveitis patients: a
565 population-based cohort study. *Eye (Lond)* **36**, 1288-1293 (2022).
566 41 Lin, H. *et al.* Differences in the prevalence of uveitis between Crohn's disease and
567 ulcerative colitis: A systematic review and meta-analysis. *Acta Ophthalmol* **102**, e485-
568 e492 (2024).
569 42 Bouma, G. & Strober, W. The immunological and genetic basis of inflammatory bowel
570 disease. *Nat Rev Immunol* **3**, 521-533 (2003).
571 43 Fuss, I. J. *et al.* Disparate CD4+ lamina propria (LP) lymphokine secretion profiles in
572 inflammatory bowel disease. Crohn's disease LP cells manifest increased secretion of IFN-
573 gamma, whereas ulcerative colitis LP cells manifest increased secretion of IL-5. *J Immunol*
574 **157**, 1261-1270 (1996).
575 44 Parronchi, P. *et al.* Type 1 T-helper cell predominance and interleukin-12 expression in the
576 gut of patients with Crohn's disease. *Am J Pathol* **150**, 823-832 (1997).
577 45 Fuss, I. J. *et al.* Nonclassical CD1d-restricted NK T cells that produce IL-13 characterize an
578 atypical Th2 response in ulcerative colitis. *J Clin Invest* **113**, 1490-1497 (2004).

579 46 Heller, F. *et al.* Interleukin-13 is the key effector Th2 cytokine in ulcerative colitis that
580 affects epithelial tight junctions, apoptosis, and cell restitution. *Gastroenterology* **129**,
581 550-564 (2005).
582 47 Strober, W. & Fuss, I. J. Proinflammatory cytokines in the pathogenesis of inflammatory
583 bowel diseases. *Gastroenterology* **140**, 1756-1767 (2011).
584 48 Sarfatis, A., Wang, Y., Twumasi-Ankrah, N. & Moffitt, J. R. Highly multiplexed spatial
585 transcriptomics in bacteria. *Science* **387**, eadr0932 (2025).
586 49 Tanoue, T. *et al.* A defined commensal consortium elicits CD8 T cells and anti-cancer
587 immunity. *Nature* **565**, 600-605 (2019).
588 50 Horai, R. & Caspi, R. R. in *Animal Models for Retinal Diseases. Neuromethods.* Vol. 46
589 207-225 (SpringerLink, 2010).
590 51 Salvador, R. *et al.* Too Much of a Good Thing: Extended Duration of Gut Microbiota
591 Depletion Reverses Protection From Experimental Autoimmune Uveitis. *Invest*
592 *Ophthalmol Vis Sci* **64**, 43 (2023).
593 52 Goux, H. J., Chavan, D., Crum, M., Kourentzi, K. & Willson, R. C. Akkermansia muciniphila
594 as a Model Case for the Development of an Improved Quantitative RPA Microbiome
595 Assay. *Front Cell Infect Microbiol* **8**, 237 (2018).
596 53 Barman, M. *et al.* Enteric salmonellosis disrupts the microbial ecology of the murine
597 gastrointestinal tract. *Infect Immun* **76**, 907-915 (2008).
598 54 Callahan, B. J. *et al.* DADA2: High-resolution sample inference from Illumina amplicon
599 data. *Nat Methods* **13**, 581-583 (2016).
600 55 Quast, C. *et al.* The SILVA ribosomal RNA gene database project: improved data
601 processing and web-based tools. *Nucleic Acids Res* **41**, D590-596 (2013).
602 56 McMurdie, P. J. & Holmes, S. phyloseq: an R package for reproducible interactive analysis
603 and graphics of microbiome census data. *PLoS One* **8**, e61217 (2013).
604 57 Mallick, H. *et al.* Multivariable association discovery in population-scale meta-omics
605 studies. *PLoS Comput Biol* **17**, e1009442 (2021).
606 58 Barnett, D. J. M., Arts, I. C. W. & Penders, J. microViz: an R package for microbiome data
607 visualization and statistics. *J Open Source Software* **6** 3201 (2021).
608 59 Peschel, S., Muller, C. L., von Mutius, E., Boulesteix, A. L. & Depner, M. NetCoMi: network
609 construction and comparison for microbiome data in R. *Brief Bioinform* **22** (2021).
610 60 McCulloch, J. A. *et al.* JAMS - A framework for the taxonomic and functional exploration
611 of microbiological genomic data. *bioRxiv* (2023).
612 61 Beghini, F. *et al.* Integrating taxonomic, functional, and strain-level profiling of diverse
613 microbial communities with bioBakery 3. *Elife* **10** (2021).
614 62 Wolock, S. L., Lopez, R. & Klein, A. M. Scrublet: Computational Identification of Cell
615 Doublets in Single-Cell Transcriptomic Data. *Cell Syst* **8**, 281-291 e289 (2019).
616 63 Wolf, F. A., Angerer, P. & Theis, F. J. SCANPY: large-scale single-cell gene expression data
617 analysis. *Genome Biol* **19**, 15 (2018).
618 64 Traag, V. A., Waltman, L. & van Eck, N. J. From Louvain to Leiden: guaranteeing well-
619 connected communities. *Sci Rep* **9**, 5233 (2019).
620 65 Aran, D. *et al.* Reference-based analysis of lung single-cell sequencing reveals a
621 transitional profibrotic macrophage. *Nat Immunol* **20**, 163-172 (2019).

Acknowledgments

We are grateful to NEI and NHLBI Flow Cytometry Cores, NEI Histology and Genetic Engineering Cores, Ms. Wuxing Yuan, Dr. Shah Rashed and members of NCI Microbiome Core, UCLA Goodman-Luskin Microbiome Center Microbiome Core, and all members of the Caspi Lab for their invaluable experimental assistance. We extend special thanks to Dr. Katsuko Sudo (Tokyo Medical University, Japan), Mr. Hirofumi Kobayashi and staff at Sankyo Labo Service Corporation, Inc. (Japan), as well as the gnotobiotic management team from NEI Veterinary Research and Resources Section for their expert support and guidance in GF and gnotobiotic colony maintenance. We also thank Dr. Eduard Ansaldo (NIAID) for sharing protocols for Akkermansia culture, Dr. Kikuji Itoh (Japan SLC, Inc.), Dr. Koji Atarashi and members of the Honda Lab for providing experimental advice. Finally, we acknowledge Dr. Geoffrey A. Mueller and staff at NIEHS Nuclear Magnetic Resonance Group for their generous assistance with metabolomics, and Drs. Kelsey Wheeler, Daniel Sellers, and Reuben Allen (Massachusetts Institute of Technology) for their insightful discussions and critical feedback. This study was supported by NIH/NEI Intramural funding, Project Number EY000184.

Author contributions

A.Z., R.H. and R.R.C. conceived and designed the study. R.R.C and R.H. supervised the project. A.Z., R.H., Y.J., A.G., S.A., and C.E.M. performed experiments and collected data. A.Z., J.H.B., Z.W., G.S., and V.N. performed computational analyses. S.H., H.N.S., J.W.L. and K.H. provided human microbiome samples, and S.K. and H.N.S. contributed to clinical interpretation. X.X., M.J.M., Z.P., B.X. provided experimental input and technical assistance. R.P. and N.M. provided technical expertise in bacteriology. J.H.B., Z.W., J.A.M., J.P.J. and C.O. contributed analytical tools, resources and expertise. A.Z. and R.H. analyzed and interpreted data and prepared figures. A.Z., R.H. and R.R.C. wrote and finalized the manuscript. All authors discussed the results, reviewed, and approved the final manuscript.

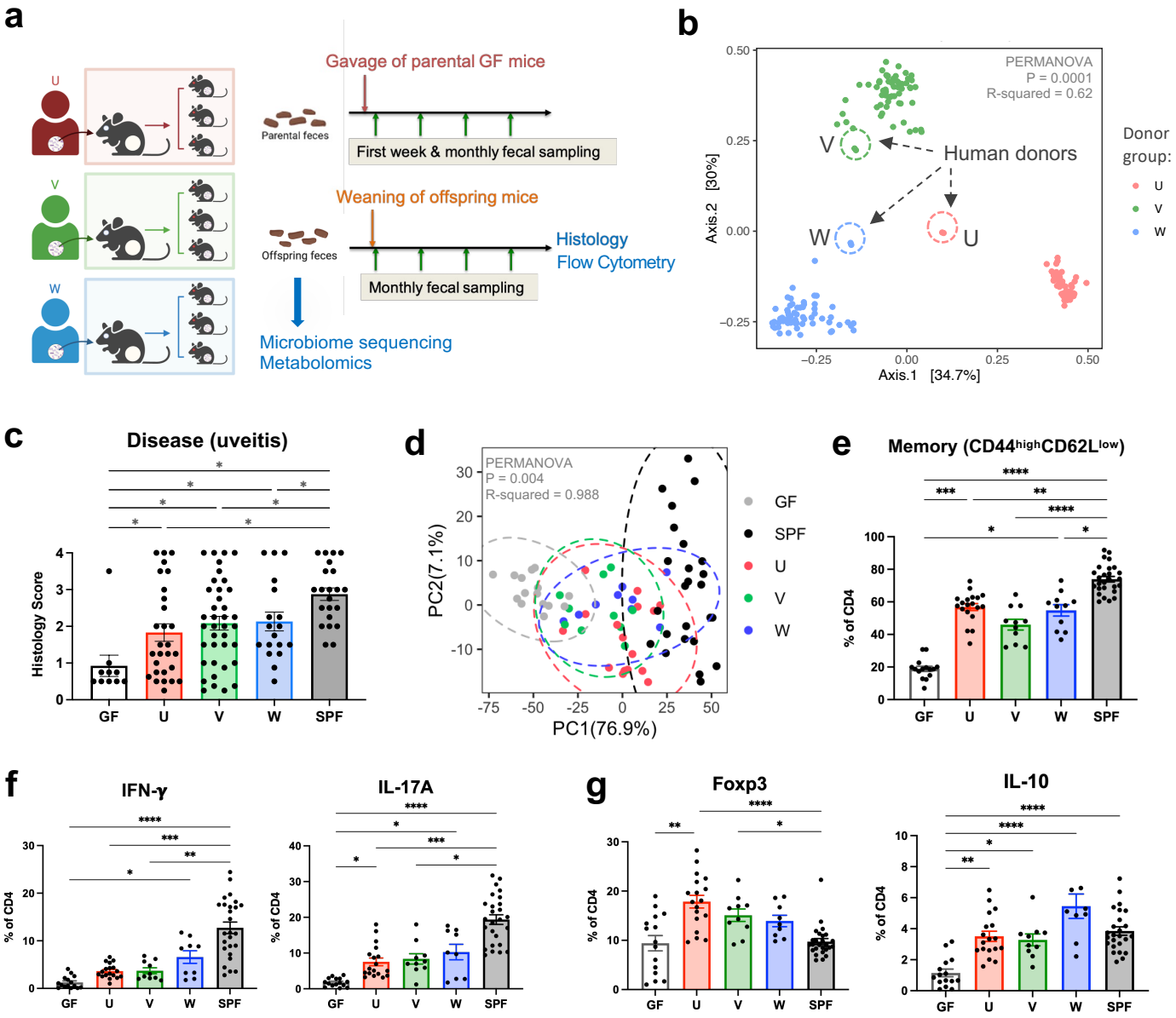

Fig. 1 | Human gut commensals support development of spontaneous experimental autoimmune uveitis (sEAU). a, Schematic representation of human fecal microbiota transfer experiments and data collection. **b**, Beta diversity based on Bray–Curtis dissimilarity showing differences in fecal microbiome composition between recipient groups U (n = 50), V (n = 59), W (n = 64). Encircled with dashed lines are the respective human donor (original) fecal samples. **c**, Disease scores (histology) of age-matched R161H mice (4-5 months old) from human flora (U, V, W, n = 28, 38, 18), SPF (n = 22) and GF (n = 10) groups (Kruskal–Wallis test between mouse recipient groups, p = 0.0002). **d**, Immunological clusters of CD4 T cells from colon lamina propria (LP) by the microbiome groups. PCA analysis performed on immune signature matrix by frequencies of CD4 T cells expressing each cell surface or intracellular marker (see **Extended Data Fig. 1e**). **e**–**g**, Frequencies of memory ($CD44^{high}CD62L^{low}$, **e**), IFN-γ- or IL-17A-producing (**f**), and regulatory (Foxp3-positive or IL-10-producing, **g**) CD4 T cells in colon LP of HuFl, SPF and GF R161H mice. **d**–**g**, Compiled data from 12 experiments, n = 15, 19, 11, 11, 27 for GF, U, V, W and SPF, respectively. Kruskal–Wallis tests show p < 0.0001 (**e**–**g**). P-values adjusted for post hoc multiple comparisons are displayed as asterisks. *P < 0.05, **P < 0.01, ***P < 0.001, ****P < 0.0001, and bar plots showing mean values ± SEMs (**c**, **e**–**g**).

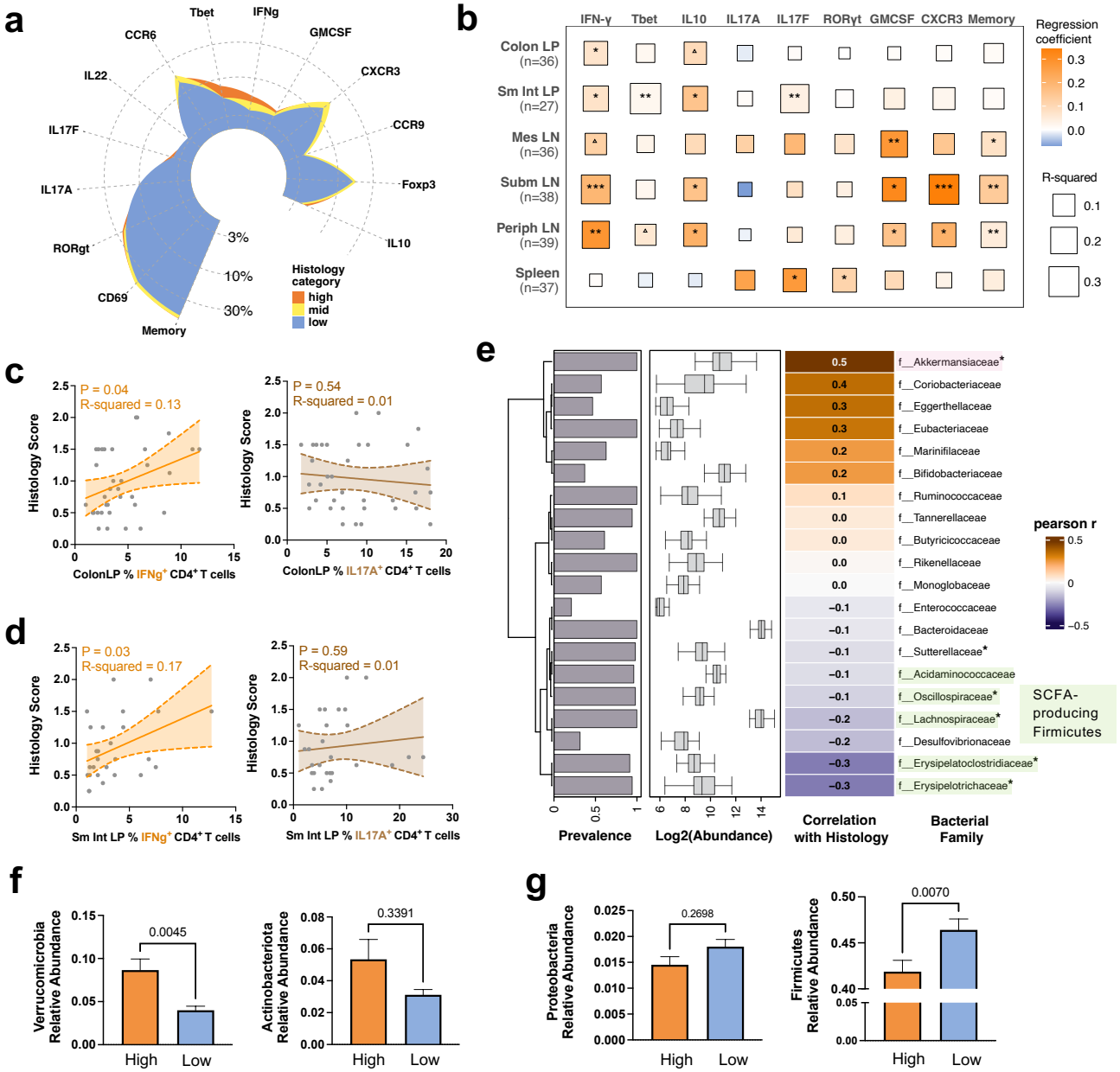

Fig. 2 | Human flora (HuFl) sEAU tracks with a dominant Th1 phenotype and abundance of Akkermansia (Verrucomicrobia). a, Mean relative frequency of colon LP CD4 T cells of each cell surface or intracellular marker arranged in a circular plot, colored by histology category: high (score ≥ 1.5, n = 10), mid (0.75 < score < 1.5, n = 8), low (score ≤ 0.75, n = 17). **b**, Correlational heatmap of histology scores with relative frequencies of each cell surface or intracellular marker in CD4 T cells across six tissue sites. LP, lamina propria; LN, lymph nodes; Sm Int, small intestine; Mes, mesenteric; Subm, submandibular; Periph, peripheral. ^0.05 < P < 0.08, *P < 0.05, **P < 0.01, ***P < 0.001, modeled by simple linear regression. **c**–**d**, Representative trend lines with 95% confidence interval (shaded area) show that disease scores of HuFl mice are positively associated with IFN-γ-producing, but not IL-17A-producing, CD4 T cells, in colon LP (**c**) and small intestine LP (**d**). Data in **a**–**d** are aggregated from 8 experiments (UVW combined, sample sizes ranged from n = 27 to 39 across tissues following quality filtering). **e**, Correlational heatmap showing major fecal bacterial taxa (out of top 20 most abundant families) that correlate with disease scores in adult HuFl R161H (UVW combined, n = 105). P-values assessed after FDR (false discovery rate) correction following Pearson correlation. *P < 0.05. **f**–**g**, More Verrucomicrobia (**f**), and fewer Firmicutes (**g**) are present in the gut of HuFl mice with high disease scores. Sample sizes are n = 36 and 43 for high and low histology categories, respectively. Data in bar plots are presented as mean values ± SEMs, and P-values from Mann-Whitney U tests are shown in plots.

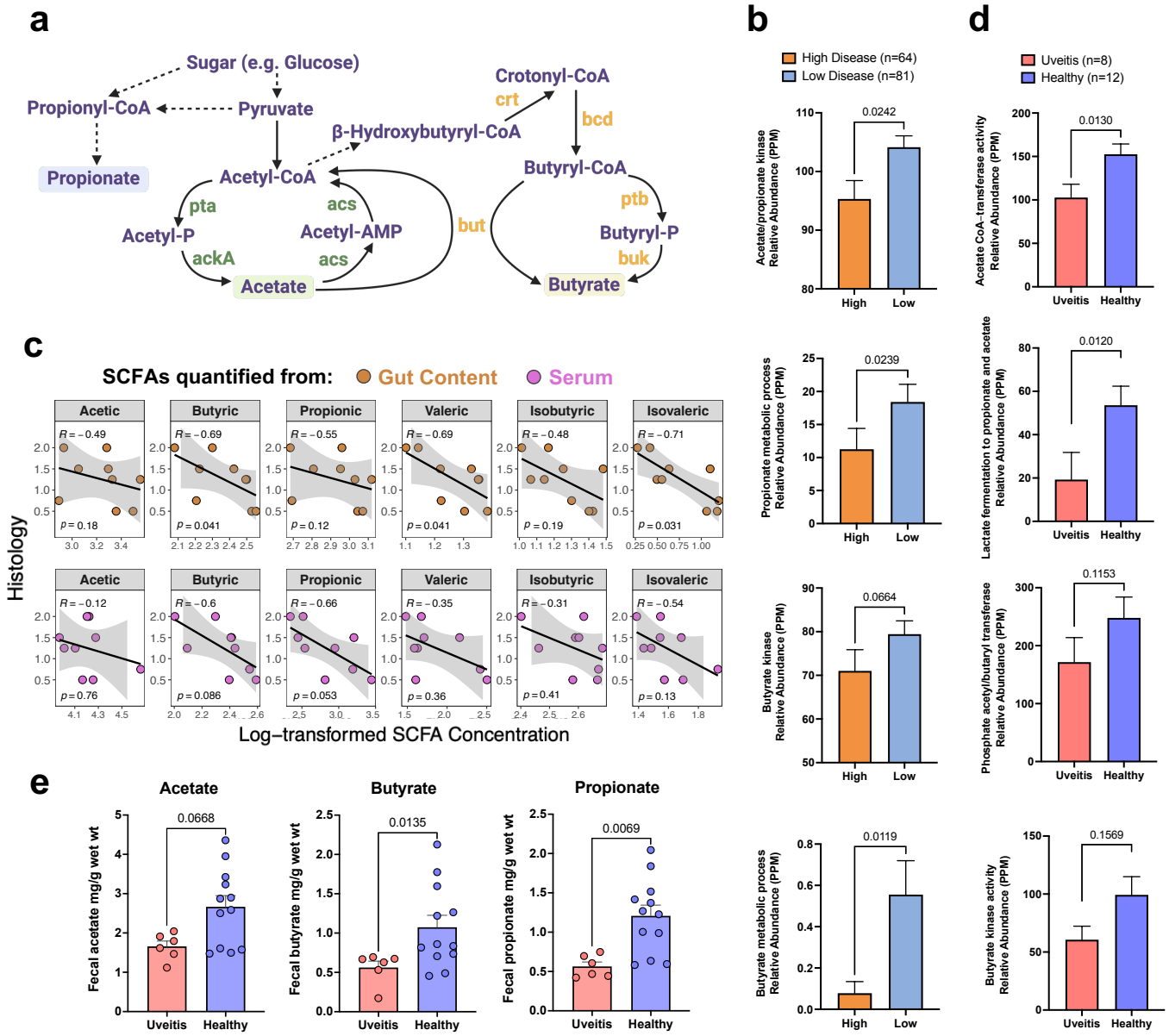

Fig. 3 | SCFA signatures are enriched in low disease HuFl mice or healthy subjects. a, A simplified pathway map highlighting functional genes involved in the main SCFA synthesis and metabolism. Dashed arrows indicate hidden intermediate steps. Abbreviations of enzyme symbols: pta, Phosphotransacetylase; ackA, Acetate kinase; acs, Acetyl-CoA synthetase; but, Butyryl-CoA:acetate CoA-transferase; ptb, Phosphate butyryltransferase; buk, Butyrate kinase; crt, Crotonase; bcd, Butyryl-CoA dehydrogenase. **b**, Enzymes in SCFA pathways (annotated with InterPro and Gene Ontology databases) are enriched in HuFl mouse gut with low histology scores (UVW combined, weanling and adult samples included). PPM, parts per million, a measure of relative abundance based on normalized base count for each feature in a metagenomic sample. **c**, Spearman correlation (visualized with a linear trend line) showing higher disease scores associated with lower SCFA concentrations both locally (in gut content) and systemically (in serum) in representative cohort U mice (n = 9). **d**, Enzymes in SCFA pathways (annotated with Gene Ontology and Pfam databases) are enriched in fecal samples from healthy humans compared to those from treatment-naïve uveitis patients, from a cohort of autoimmune uveitis (ocular-restricted, including idiopathic uveitis, VKH/SO and BCR). Sex, age, race and diet are comparably represented in patient and control groups. Normalized gene abundance is reported in PPM. **e**, SCFA levels from uveitis patients and healthy controls (same cohort as in **d,** but n = 6 available from the patient group). For **b, d** & **e**, Data are presented as mean values ± SEMs. Statistical significance was determined by Mann-Whitney U test.

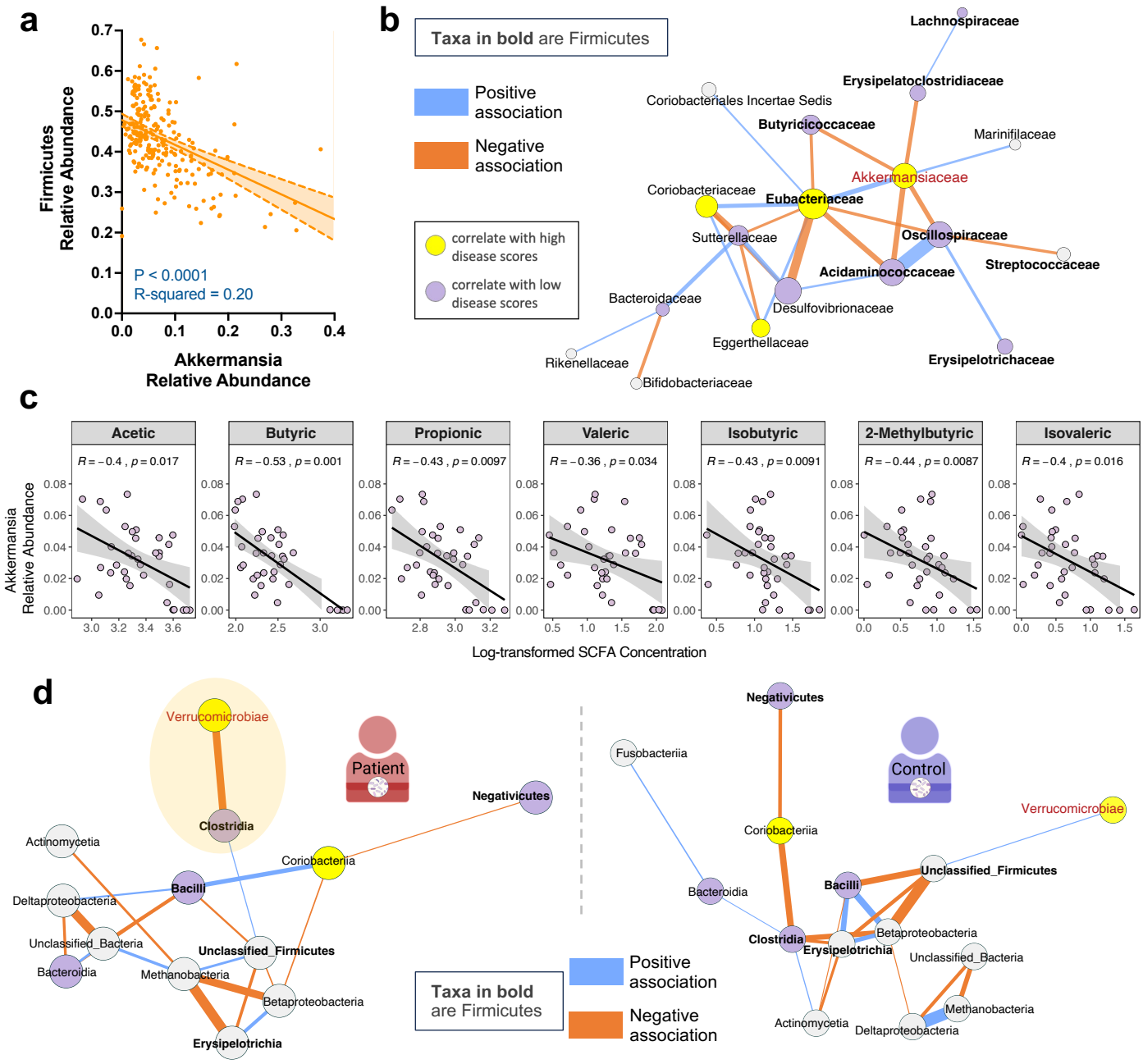

Fig. 4 | Akkermansia negatively correlates with Firmicutes in both sEAU and clinical uveitis. a, Simple linear regression showing a negative correlation of microbial relative abundance between Akkermansia (equivalent to Verrucomicrobia in this dataset) and Firmicutes in HuFl R161H mice (n = 234, UVW combined, weanling and adult samples included). **b**, Fecal bacterial association network exemplified in HuFl cohort V (n = 79, weanling and adult samples included). Network constructed at the taxonomic level of the bacterial family. Correlations with a threshold of Pearson r > 0.5 were transformed into dissimilarities via the "unsigned" distance metric, on which edge weights (strength of correlations) are based. Blue edges correspond to positive associations and orange edges to negative ones. Yellow and purple nodes represent taxa enriched in high *vs.* low disease categories, with Firmicutes labeled as bolded taxon names. Bigger nodes are more influential in the network (higher eigenvector centrality). **c**, Spearman correlation (visualized with a linear trend line) showing a negative association between relative Akkermansia abundance and SCFA concentrations in R161H gut (n = 35, UVW and SPF combined). Akkermansia was selected following multivariable association between SCFA concentrations and microbial features using MaAsLin2. **d**, Class level association networks in treatment-naïve uveitis patients (left, n = 8) and healthy controls (right , n = 12) from the same cohort of autoimmune uveitis. Correlations with a threshold of Pearson r > 0.3 are shown. Node and edge color schemes same as in **b**. Shaded ellipse in the patient network highlights the negative correlation between Verrucomicrobiae (Akkermansia) and Clostridia (Firmicutes), and this relationship is absent from the healthy human gut.

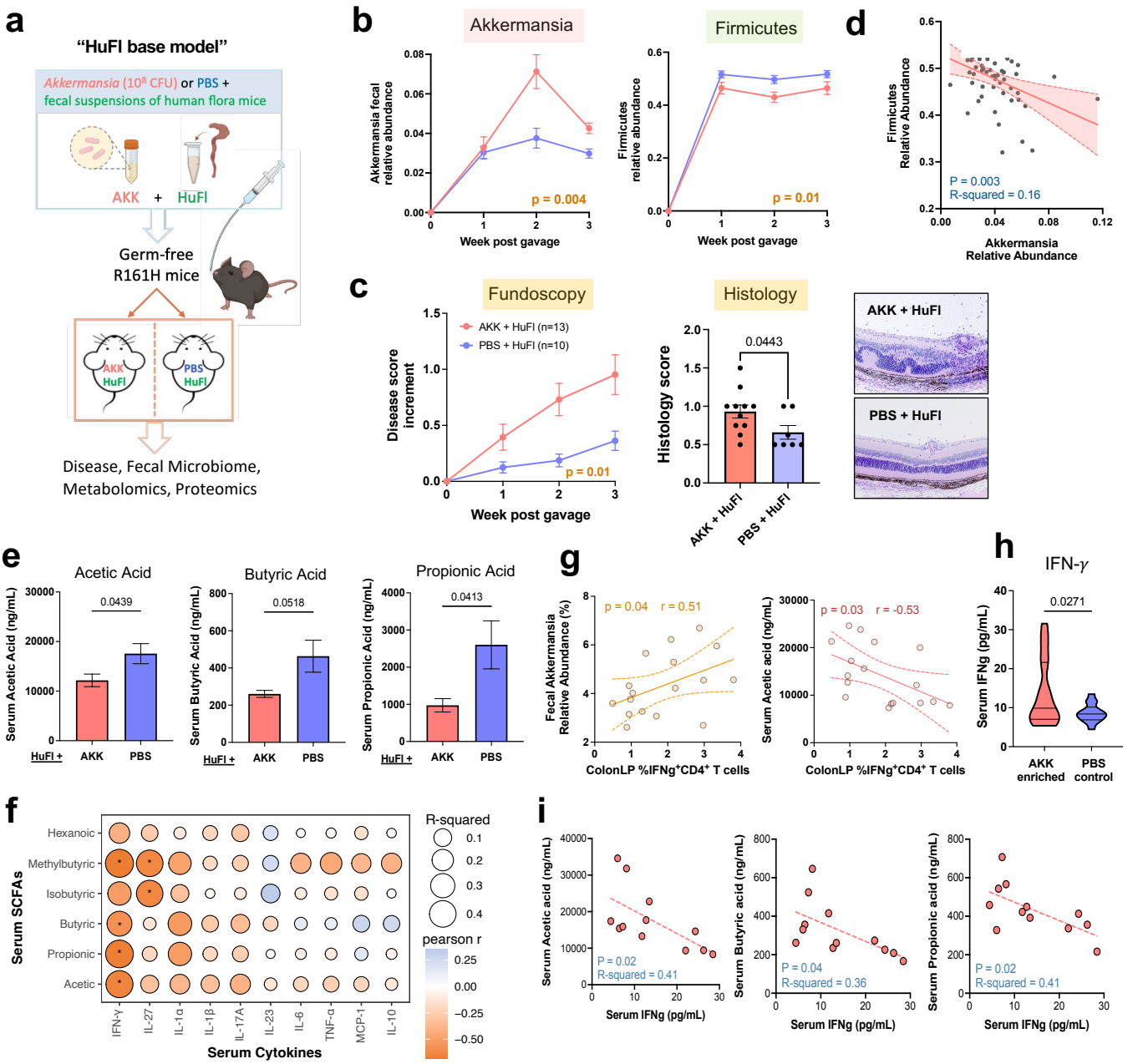

Fig. 5 | Akkermansia promotes uveitis by outcompeting SCFA producers and decreasing circulating SCFA levels. **a**, Study design of microbe reconstitution experiments. Previously GF R161H mice gavaged with a baseline human gut microbiota suspension (HuFl) plus *A. muciniphila* culture (AKK, 10^8 CFU) or sterile PBS. **b**, Relative abundance of Akkermansia and Firmicutes in feces from one representative of 3 experiments (n = 7 and 6 for Akk-rich and control, respectively). **c**, Left: Fundoscopy score increments from starting disease scores, combined from three experiments. Right: Histology scores and example images from 2 out of 3 experiments (n = 11 and 7 for Akk-rich and control, respectively). Mean values ± SEM. P-value determined by Welch-corrected t test. **d**, A negative correlation of relative abundance between Akkermansia and Firmicutes (n = 52, AKK and PBS groups combined, multiple time points included) by simple linear regression. **e**, Serum concentrations of main SCFAs are significantly lower in Akk-rich (n = 13) mice than in PBS controls (n = 10). Serum harvested 3 – 4 weeks post gavage, three experiments combined. **f**, Correlational heatmap of SCFA levels with cytokine concentrations in serum of engrafted mice. *P < 0.05, modeled by simple linear regression as well as Pearson correlation. **g**, Spearman correlation (visualized with a linear trend line) showing Akkermansia relative abundance associated positively, and serum acetic acid associated negatively, with the frequency of IFN-γ-producing CD4 T cells in colonic LP. **h**, Akk-enriched (n = 18) mice had higher serum IFN-γ concentrations compared to PBS control mice (n = 14), five experiments combined, of which two experiments used the minimal flora model. **i**, Representative trend lines show that main SCFA concentrations are negatively associated with IFN-γ levels in serum. Data in **g, i** are from 2 experiments (n = 12) using the minimal flora model.

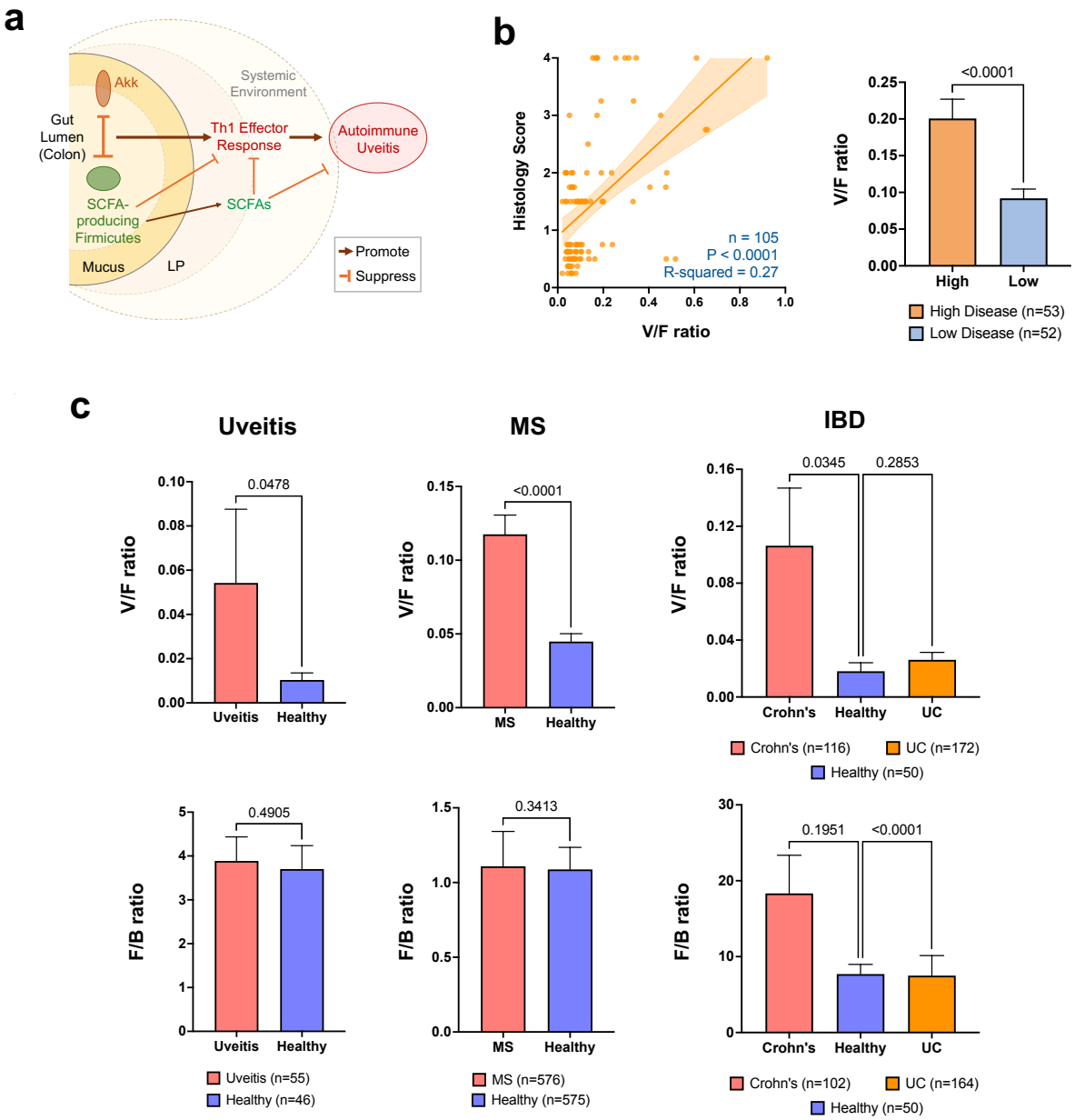

Fig. 6. **The inverse relationship between Verrucomicrobia and Firmicutes extends to clinical uveitis, multiple sclerosis (MS) and Crohn's disease. a**, Graphical summary of the working model. **b**, A positive correlation between V/F (Verrucomicrobia/Firmicutes) ratios and histology scores of HuFl mice by simple linear regression, and V/F ratios compared between high and low disease of HuFl mice. **c**, V/F and F/B (Firmicutes/ Bacteroidetes) ratios compared between patients from uveitis, MS and IBD and their respective healthy controls. Analyzed datasets of MS and IBD (Crohn's disease and UC) and healthy controls were from public sources. Uveitis and MS cohorts included those established on treatment. For F/B ratio in the IBD cohort, samples with <0.1% relative abundance of either Bacteroidetes or Firmicutes were removed from the analysis. Data are presented as mean values ± SEM. Statistical significance was determined by Mann-Whitney U test (one-tailed analysis was applied for uveitis and MS) and Kruskal–Wallis test with P-values adjusted for post hoc multiple comparisons (for IBD).